

# Optimal design of structured nanospheres for ultrasharp light-scattering resonances as molecular imaging multilabels

Kun Chen  
Yang Liu  
Guillermo Ameer  
Vadim Backman

Northwestern University  
Department of Biomedical Engineering  
Evanston, Illinois 60208  
E-mail: v-backman@northwestern.edu

**Abstract.** Optical molecular imaging could potentially enable noninvasive high-resolution characterization and diagnosis of living tissue. The capability to image multiple molecular targets simultaneously is particularly important. Currently this task cannot be achieved using conventional optical contrast agents, due to their broad spectral responses (~80 to 200 nm). Developments in research on semiconductor nanocrystals (quantum dots) provide one possible solution. We describe a different concept of multilabel molecular imaging that utilizes resonant light-scattering spectroscopy of multilayered nanospheres to achieve tunable ultrasharp resonance peaks with widths as narrow as 10 nm. Our theoretical study demonstrates that dozens of molecular targets can potentially be imaged simultaneously using this approach. © 2005 Society of Photo-Optical Instrumentation Engineers. [DOI: 10.1117/1.1899684]

**Keywords:** multilabel molecular imaging; multilayered nanospheres; resonant light-scattering spectroscopy.

Paper 04022 received Feb. 23, 2004; revised manuscript received Jun. 15, 2004; accepted for publication Aug. 17, 2004; published online Apr. 29, 2005.

## 1 Introduction

It is now recognized that the field of nanophotonics may revolutionize biology and medicine by enabling novel methods of molecular imaging, analyte detection, and drug delivery.<sup>1,2</sup> An important component of nanophotonics has been the use of metallic nanoparticles due to their remarkable optical properties. The spectra of light scattered by such nanoparticles exhibit resonances at visible and near-IR (NIR) wavelengths, which may enable their use as molecular contrast agents in various modalities of optical imaging of living tissue, such as light-scattering spectroscopic (LSS) imaging. We have already shown the capabilities of LSS imaging<sup>3,4</sup> to provide accurate, hitherto unattainable information about tissue microarchitecture at scales ranging from tens of nanometers to tens of micrometers.<sup>3-6</sup> Furthermore, we showed that LSS imaging could be used for noninvasive imaging and detection of early stages of precancer and other diseases associated with alteration of tissue structure. By utilizing metallic nanoparticles as contrast agents in LSS imaging, not only the information concerning tissue structure but also its molecular composition can be obtained. Thus, noninvasive multilabel molecular imaging of living tissue could potentially be achieved using LSS imaging. Such a technique can be used not only for tissue molecular imaging, but also for detection of multiple analytes and the biochemical analysis of materials.

Sharp and symmetric fluorescence peaks generated by quantum dots (QDs) have been explored by several groups to achieve the goal of multicolor labeling.<sup>7-12</sup> Recently, several

problems associated with QDs, such as fluorescence quenching, nonspecific binding, and aggregation, have been solved. Compared with organic fluorophores, QDs have several unique optical properties. The fluorescence spectra of QDs are narrow, symmetric and tunable by varying the size of QDs. Because QDs can be excited at any wavelength shorter than the emission maximum, a single excitation wavelength can be used to induce fluorescence from a mixture of different sized QDs. In addition, the narrow fluorescence spectra enable multiple targets to be detected and resolved simultaneously. Thus, after tagging different sized QDs to different molecular targets, multicolor labeling can be implemented. Thus, in applications where fluorescence imaging is desirable and feasible, QDs provide an efficient solution to obtain molecular imaging. However, for broadband, e.g., white light, light scattering imaging, such as LSS imaging,<sup>3,13-15</sup> optical coherence tomography<sup>16</sup> (OCT), differential pathlength spectroscopy,<sup>17,18</sup> and polarization imaging,<sup>19,20</sup> alternative contrasts are required. Recently, this has led to a significant interest in the use of metallic nanoparticles and nanoshells as such contrast agents.

Resonant light scattering, arising from plasmon resonance in structured metallic nanoparticles, are superior to conventional optical methods for diagnostic detection and labeling in several aspects. The photoefficiency of a gold nanoparticle can be equivalent to as many as hundreds of thousands of fluorescent molecules.<sup>21</sup> Furthermore, the stability of metallic nanoparticle properties makes resonant light scattering immune to time-dependent blinking or photobleaching.<sup>21,22</sup>

Address all correspondence to Dr. Vadim Backman, Northwestern University, Department of Biomedical Engineering, Evanston, Illinois 60208.

Moreover, metallic nanoparticles can be conjugated with antibodies, DNA probes, ligands, and protein receptors,<sup>21–24</sup> which enables using nanoparticles as molecular labels. Sokolov et al.<sup>25</sup> utilized this property of solid gold and silver nanospheres in a single-label confocal reflectance imaging of living epithelial cells. However, because solid metallic nanoparticles have relatively wide resonance peaks, only a few such peaks can be resolved simultaneously. Therefore, multi-color labeling may not be achieved within the range from the visible to the NIR, and novel nanoscale agents with sharp and easily controllable resonances must be developed. We propose herein a novel concept that utilizes nanoparticle engineering to facilitate multilabel molecular imaging of tissue, which is based on the resonant light scattering by multilayered metallic nanospheres.

## 2 Methods

A thorough, systematic investigation of resonant light scattering by structured metallic nanoparticles can provide deep insight into this phenomenon and guide the optimal design of the nanoparticle structures. Studies of particles with arbitrary shapes must resort to time-consuming, purely numerical computations, whereas analytical expressions have been well established for concentric spherical shells. For practical applications, spheres are the most natural shape and the easiest to synthesize and control, and thus have by far received the most attention. Up to now, efforts have been focused only on solid metallic nanospheres and two-layered nanoshells, because of the availability of robust codes for Mie scattering and coated-sphere scattering. The general case of nanospheres with an arbitrary number of layers and an arbitrary combination of materials has so far been avoided due to computational complexity. Nevertheless, we managed to overcome this barrier and developed an accurate numerical model of resonant light scattering of multilayered nanospheres based on the exact solution of Maxwell's equations (to be posted on the Internet as a publicly accessible code). To accomplish this, we implemented the robust and highly efficient recurrence algorithm introduced by Wu and Wang<sup>26</sup> to calculate the exact solutions to Maxwell equations of light scattering by multilayered concentric spheres.

The required inputs to our computational experiments are the refractive index  $n(\lambda) + ik(\lambda)$  of the material at each layer and the layer's dimension (the radius of the core or the thickness of a shell). The imaginary part of the refractive index [e.g.,  $k(\lambda)$ ] is proportional to the absorbance spectrum of the material. An enormous number of combinations can be explored as each structured nanosphere is characterized by the number of layers, the choice of material for each layer, and each layer's size. Here, we report results on two- and three-layered nanospheres consisting of gold, silver, and silica. Extension to other metals is straightforward. The scattering efficiency  $Q_{\text{sca}}(\lambda)$  is calculated using the refractive indices measured on evaporated films of gold and silver.<sup>27</sup> The total scattering cross section  $\sigma_{\text{sca}}$  is proportional to  $Q_{\text{sca}}$ , i.e.,  $\sigma_{\text{sca}} = \pi a^2 Q_{\text{sca}}$ , where  $a$  is the overall radius of the sphere. Because for single scattering events, the intensity of light scattered by a nanosphere is proportional to  $Q_{\text{sca}}$ , knowing the scattering cross section is sufficient for imaging in the backward geometry. In the case of imaging based on multiple

scattering events, as in deep tissue imaging, the extinction cross section  $\sigma_{\text{ext}}$  must be used. Note that  $Q_{\text{sca}}$  does include the effect of light absorption by the nanosphere materials, due to the nonzero  $k(\lambda)$ .

## 3 Results and Discussion

In this paper, we describe a theoretical basis of nanoparticle engineering to facilitate multilabel molecular imaging of tissue, which is based on the resonant light scattering by multilayered metallic nanospheres. This scheme may potentially enable imaging of multiple molecular targets simultaneously over a wide image area. Here, a spectrum of light scattering is collected for each pixel in the imaged field. Then, the spatial distribution of each molecular target is represented by the spatial distribution of nanoparticles, which in turn is reported by the presence and/or absence of its resonant light scattering peak at each pixel. Unlike the QD fluorescence approach, LSS imaging using multilayered metallic-dielectric nanospheres does not utilize UV excitation to access the full visible-NIR range. Furthermore, the biocompatibility of the multilayered nanospheres should be determined by the outer shell material and should be similar to gold or silver nanoparticles, whose dynamics in tissue including delivery, toxicity, and clearance have been extensively studied.<sup>28–32</sup> Because gold nanoparticles have been applied in the study for drug delivery,<sup>28,29</sup> adoption of this kind of nanospheres in human tests is expected to be faster.

To achieve multilabel molecular imaging, the structure of the engineered metallic nanospheres should possess the following optical properties: a prominent resonance peak with a narrow width characterized by the full width at half maximum (FWHM), a high resonance-to-baseline ratio, and easy tunability of the spectral position of the resonance by simple variation of the nanosphere configuration. Accordingly, a series of distinguishable resonances can be arranged to cover the visible-NIR wavelength range. Because each characteristic resonance peak is used to label a specific molecular target, the maximal number of contrast agents  $N$  is approximately  $N = \Delta\lambda/\text{FWHM}$ , where  $\Delta\lambda$  is the wavelength range of detection. For example, when  $\text{FWHM} = 16$  nm, we anticipate  $\sim 37$  resonance peaks can be distinguished in the wavelength range from 400 to 1000 nm; thus,  $\sim 37$  targets can be detected at the same time, if necessary.

Importantly, one of the major complications arising in imaging of turbid media, such as tissues, is the strong background of endogenous light scattering, which itself possesses spectral variations. These broad spectral features are used in LSS imaging to obtain important information about tissue structure. Because endogenous light scattering spectra and nanoparticle resonances may interfere with each other, resonances with sufficiently narrow FWHMs and high peak-to-baseline ratios are critical for discrimination. Nevertheless, in light of the preceding requirements, previously described metallic nanoparticles do not lend themselves for multilabeling.

Regarding the tunability criterion, studies have shown<sup>33–35</sup> that resonant light extinction by metallic nanoparticles has a strong dependence on nanoparticle size, shape, and material composition. Averitt et al.,<sup>36</sup> Halas et al.,<sup>37</sup> and Jackson and Halas<sup>38</sup> showed that extinction resonances in two-layered nanoshells, i.e., concentric nanospheres consisting of a dielec-

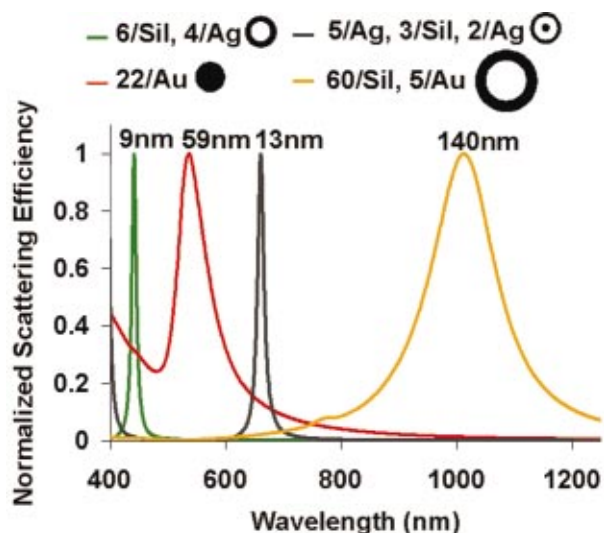


**Fig. 1** Comparison of resonant light scattering peaks for solid, two- and three-layered nanospheres. The peak values are normalized to unity. The values of the peak FWHMs are listed on top of each curve. The sphere structure is denoted in the legend as core radius/core material; thickness of shell 1/material of shell 1; thickness of shell 2/material of shell 2 (for three-layered nanospheres). All dimensions are in nanometers. Ag stands for silver; Au, for gold; and Sil, for silica. The schematic on the right illustrates the four types of nanoparticles (not shown to scale). Black color shows nanoparticle layers composed of either silver or gold. White color shows nanoparticle layers composed of silica.

tric core and a metal shell, can be precisely controlled in the visible-NIR spectral range by varying the core-to-shell ratio. Loo et al.<sup>16</sup> showed the feasibility of utilizing two-layered nanoshells for *in situ* tissue imaging. Although these studies demonstrate the tunability of two-layered nanoshells, the effort has been mostly devoted to investigating the properties of relatively large nanoshells (tens to hundreds of nanometers in diameter), which give rise to resonances with spectral widths typically from 150 to 200 nm (Fig. 1). This width range enables the use of only three to four distinct biomarkers in the whole visible-NIR range and would interfere with endogenous spectral features, as described earlier. Moreover, the delivery of such large nanoparticles to target sites in living tissues could prove difficult. In addition, these studies focused on the tunability of light extinction, which is dominated by light absorption, rather than resonant light scattering.

In previously reported molecular imaging experiments,<sup>25</sup> solid metallic nanoparticles (sizes  $\sim 10$  nm) were used. However, FWHMs of solid nanosphere resonances are typically wide ( $\sim 60$  nm), and the peak-to-baseline ratio is only  $\sim 3$  to 5 (Fig. 1). Furthermore, although their resonance positions can be controlled by varying their size, this approach is not effective due to a weak dependence of resonance position on particle size. Tuning resonance peak positions by varying particle sizes may also limit their use for tissue imaging, because nanospheres of different sizes have different rates of diffusion within a tissue. As a result, the accurate mapping of the concentrations of the target molecules by the nanospheres will be distorted.

First, to validate our algorithm, we compared the predictions of our computational model for silica-core silver-shell

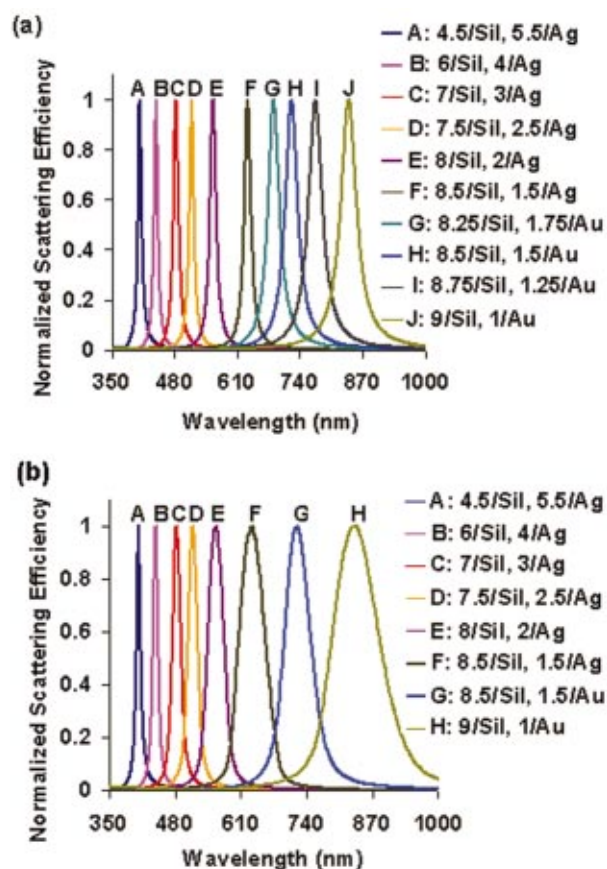


**Fig. 2** Resonant light scattering peaks of two-layered nanospheres with silica cores. The sphere structure is denoted in the legend as core radius/core material; thickness of the shell/material of the shell. All dimensions are in nanometers. Ag stands for silver; Au, for gold; and Sil, for silica. (a) The overall radius of nanospheres fixed at 10 nm, and the relative dimension of the core versus the shell is varied. Consequently, the resonance position can be controlled to cover the entire visible-NIR range. The core radius has no size distribution. The FWHMs of the peaks are, from left to right, 9, 9, 12, 11, 15, 16, 29, 31, 35, and 40 nm, respectively. (b) The silica core radius carries a  $\pm 5\%$  size distribution. The FWHMs of the peaks are, from left to right, 10, 12, 20, 22, 37, 58, 47, 60, 77, and 106 nm, respectively. As expected, the size distribution broadens the resonance peaks.

nanoshells of various sizes with the experimental results previously obtained by Oldenburg et al.<sup>33</sup> and Jackson and Halas<sup>38</sup> were found to be in an excellent agreement (case B in Fig. 1). Then, we utilized our model to investigate light scattering and absorption properties of multilayered nanoshells. Figure 1 shows the typical resonance scattering spectra for nanospheres of four different configurations. Both the solid gold nanosphere ( $a=22$  nm) and the large two-layered nanoshell with a 60-nm silica core and a 5-nm gold shell produce wide resonance peaks. On the other hand, specially configured two- and three-layered nanospheres are capable of producing ultrasharp resonances with spectral widths of the order of 10 nm and significantly improved peak-to-baseline ratios.

Our results indicate that in two-layered nanoshells, the spectral position of resonant peak depends on the core-to-shell ratio [Fig. 2(a)]. This result agrees with the observation of Oldenburg et al.<sup>33</sup> made for larger nanoshells. As shown in

Fig. 2(a), the spectral position of the resonance can be precisely controlled throughout the visible-NIR range. (As in case of all nanoparticles, certain physical effects such as nanoparticle aggregation, electron impurity and defects, as well as electron-interface, electron-electron, and electron-lattice collisions, may potentially affect the shape of the resonance peaks. Although nanoparticle aggregation can be inhibited by using surfactants and these effects were not found to significantly affect the nanoparticle resonances, future experiments will enable a thorough understanding of the factors that may affect the resonances generated by structured nanospheres in various environments.) In Fig. 2(a), all nanoparticle configurations share the same overall size of 10 nm in radius, and the resonance position is varied depending on the relative dimensions of the nanoparticle layers. As the resonance shifts to longer wavelengths, the FWHM monotonically increases. Because the synthesis of nanoparticles with a size distribution below 5 to 10% is difficult to achieve, we investigated the influence of the size distribution on the resonance width. We modeled  $\pm 5\%$  variation in the radius of the silica core. As expected, a finite distribution of the nanosphere sizes broadens the resonance peaks, particularly at longer wavelengths [Fig. 2(b)]. Therefore, the difficulty of synthesizing monodisperse silica cores (especially below  $\sim 100$  nm) may limit the use of this type of nanoshells for multilabel molecular imaging at the present stage.

Although the synthesis of nanoscale silica cores below 100 nm has been difficult, the synthesis of silica-coated metallic nanoparticles with accurately controllable dimensions has been achieved experimentally for overall diameters below 100 nm. For example, recently, Liz-Marzan et al. successfully coated silica on metallic nanoparticles.<sup>39</sup> Although the resonances obtained using such metal-core silica-shell nanoparticles suffer from similar problems as those of solid metallic nanoparticles, these nanoshells can serve as basis to obtain ultrasharp and tunable resonant peaks, as described in the following.

Here we report, for the first time, theoretical evidence that three-layered nanospheres, which can be easily synthesized using current methods,<sup>40–46</sup> have improved properties as multicolor labels, compared with existing resonant light scattering markers, including solid metallic nanoparticles and two-layered nanoshells. The three-layered nanospheres consist of alternating layers of metallic and dielectric materials, e.g., metallic-core and silica-shell nanoparticles coated with another layer of a metal. The basic building blocks of such three-layered nanospheres have been readily and extensively synthesized within the past decade.<sup>40–47</sup> Specifically, a series of nanospheres with a silver core, silica middle shell, and silver or gold surface shell can replicate the array of sharp resonances similar to the two-layered nanoshells of Fig. 2 throughout the entire visible-NIR region [Fig. 3(a)]. According to Rayleigh criterion, up to  $N \sim 30$  resonance peaks can be distinguished simultaneously. In turn, this may enable parallel imaging of up to 30 distinct biomarkers simultaneously. Remarkably, the widths of these resonances are much less sensitive to statistical size variations [Fig. 3(b)]. For example, Fig. 3(b) compares the increase of the resonance FWHMs with the standard deviation of the size distribution of the silica layer for two- and three-layered nanospheres, respectively. According to the model, the FWHMs of the resonances for

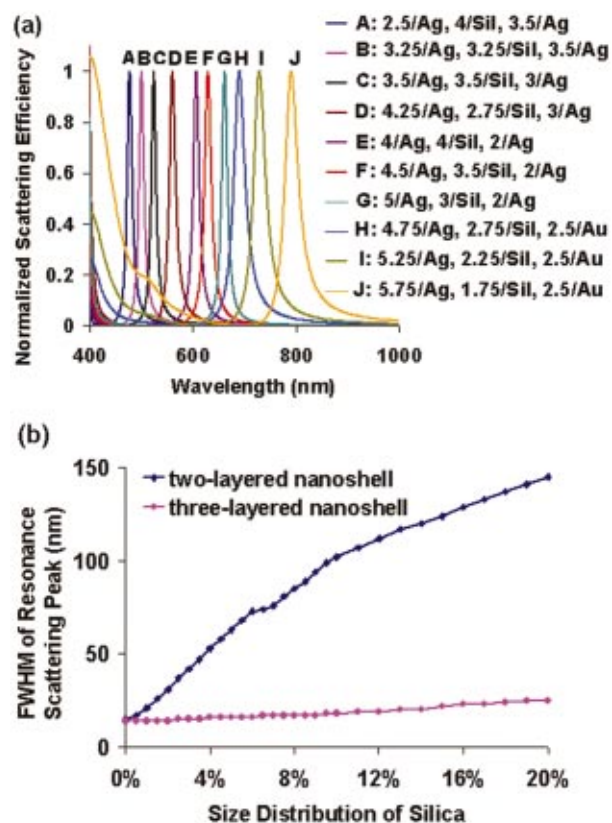


**Fig. 3** Resonant light scattering of three-layered nanospheres. (a) The overall radius of the spheres is fixed at 10 nm. The spheres consist of a silver core, a silica middle shell, and a silver/gold surface shell. The sphere structure is denoted in the legend as core radius/core material; thickness of shell 1/material of shell 1; thickness of shell 2/material of shell 2. All dimensions are in nanometers. Ag stands for silver; Au, for gold; and Sil, for silica. Sharp resonant peaks of the spheres can be tuned to cover the visible-NIR wavelength range by varying the sphere structure configurations. The presented curves are obtained without a size distribution of silica layer. The FWHMs of the peaks are, from left to right, 12, 12, 11, 14, 14, 15, 13, 26, 28, 29, 31 nm, respectively. According to Rayleigh criterion, up to  $N \sim 30$  resonance peaks can be distinguished simultaneously. (b) The dependence of the FWHMs of the resonance peaks on the size distribution of a silica layer.

two-layered nanospheres increase dramatically with standard deviation, whereas the FWHMs of three-layered nanospheres show only a weak dependence on standard deviation.

Clearly, nanospheres will exhibit both scattering and absorption features. Light absorption due to multiple interactions (absorptions and/or scatterings) by nanospheres may complicate their applications in deep tissue imaging. However, about 85% of all cancers originate in the epithelial level, and it is the photons single-scattered in the backward direction by this superficial tissue that carry the most diagnostic information.<sup>3,13–15,17</sup> Multiple-scattered photons must be rejected via experimental design or theoretical modeling. In this scenario, the single-scattering signal from nanospheres is proportional to the scattering cross section that is investigated in this paper. However, in deep tissue imaging, where the effect of multiple light scattering becomes important, extinction cross section must also be taken into account.

We presented a new scheme for multicolor molecular imaging and a mathematical model-based approach to systematically guide the experimental design of nanoparticles. These kinds of nanoparticles have proven biocompatibility, and since nanogold has been used in drug delivery in humans, the pace of their applications is expected to be faster than other agents. In addition, because only the visible to NIR wavelength range is used, the potential harm of UV radiation to the human body is avoided. Ultrasharp light scattering resonances generated by structured nanospheres may potentially facilitate imaging of a wide range of molecular signatures of various diseases and monitoring of molecular events for tissue and material engineering applications. Although initially designed for LSS imaging, ultrasharp resonances generated by the structured nanospheres will likely enhance the role and impact of nanophotonics on other disciplines. In particular, many modalities of optical imaging including optical coherence tomography (OCT) and confocal microscopy may see an immediate benefit. Moreover, the molecular characterization of tissue by means of resonant light scattering may compliment other approaches, such as those based on the achievements in the field of QD fluorescence.<sup>7-12</sup> Furthermore, the approach reported here may facilitate the identification of novel optimal configurations of nanoparticles for specific material, biological, medical, or engineering applications. Experimental studies aimed to synthesize multilayered nanoparticles to validate the model presented herein and utilize their resonant properties for LSS molecular imaging of tissue are currently underway in our group.

#### Acknowledgment

This work was supported in part by the Institute for Bioengineering and Nanotechnology in Advanced Medicine and National Institutes of Health (NIH) Grant No. 1R21EB003454-01.

#### References

1. M. L. Brongersma, "Nanoshells: gifts in a gold wrapper," *Nat. Mater.* **2**, 296–297 (2003).
2. J. Yguerabide and E. E. Yguerabide, "Light-scattering submicroscopic particles as highly fluorescent analogs and their use as tracer labels in clinical and biological applications—II. Experimental characterization," *Anal. Biochem.* **262**, 157–176 (1998).
3. V. Backman, M. B. Wallace, L. T. Perelman, J. T. Arendt, R. Gurjar, M. G. Muller, Q. Zhang, G. Zonios, E. Kline, T. McGillican, S. Shapshay, T. Valdez, K. Badizadegan, J. M. Crawford, M. Fitzmaurice, S. Kabani, H. S. Levin, M. Seiler, R. R. Dasari, I. Itzkan, J. Van Dam, and M. S. Feld, "Detection of preinvasive cancer cells *in situ*," *Nature* **406**, 35–36 (2000).
4. R. S. Gurjar, V. Backman, L. T. Perelman, I. Georgakoudi, K. Badizadegan, I. Itzkan, R. R. Dasari, and M. S. Feld, "Imaging of human epithelial properties with polarized light scattering spectroscopy," *Nat. Med.* **7**, 1245–1248 (2001).
5. V. Backman, V. Gopal, M. Kalashnikov, K. Badizadegan, R. Gurjar, A. Wax, I. Georgakoudi, M. Mueller, C. W. Boone, R. R. Dasari, and M. S. Feld, "Measuring cellular structure at submicron scale with light scattering spectroscopy," *IEEE J. Sel. Top. Quantum Electron.* **7**, 887–894 (2001).
6. K. Chen, A. Kromine, M. P. Ulmer, W. B. Wessels, and V. Backman, "Determination of nanoparticle sizes beyond the diffraction limit using UV light scattering spectroscopy," *Opt. Commun.* **228**, 1–7 (2003).
7. M. Y. Han, X. H. Gao, J. Z. Su, and S. M. Nie, "Quantum-dot-tagged microbeads for multiplexed optical coding of biomolecules," *Nat. Biotechnol.* **19**, 631–635 (2001).
8. X. H. Gao and S. M. Nie, "Molecular profiling of single cells and tissue specimens with quantum dots," *Trends Biotechnol.* **21**, 371–373 (2003).
9. J. K. Jaiswal, H. Mattoussi, J. M. Mauro, and S. M. Simon, "Long-term multiple color imaging of live cells using quantum dot bioconjugates," *Nat. Biotechnol.* **21**, 47–51 (2003).
10. B. Ballou, B. C. Lagerholm, L. A. Ernst, M. P. Bruchez, and A. S. Waggoner, "Noninvasive imaging of quantum dots in mice," *Bioconjugate Chem.* **15**, 79–86 (2004).
11. B. Dubertret, P. Skourides, D. J. Norris, V. Noireaux, A. H. Brivanlou, and A. Libchaber, "In vivo imaging of quantum dots encapsulated in phospholipids micelles," *Science* **298**, 1759–1762 (2002).
12. Z. Kaul, T. Yaguchi, S. C. Kaul, T. Hirano, R. Wadhwa, and K. Taira, "Mortalin imaging in normal and cancer cells with quantum dot immuno-conjugates," *Cell Res.* **13**, 503–507 (2003).
13. H. K. Roy, Y. Liu, R. K. Wali, Y. Kim, M. J. Goldberg, A. K. Kromine, and V. Backman, "Four-dimensional elastic light scattering fingerprints as preneoplastic markers in the rat model of colon carcinogenesis," *Gastroenterology* **126**, 1071–1081 (2004).
14. L. T. Perelman, V. Backman, M. Wallace, G. Zonios, R. Manoharan, A. Nusrat, S. Shields, M. Seiler, C. Lima, T. Hamano, I. Itzkan, J. Van Dam, J. M. Crawford, and M. S. Feld, "Observation of periodic fine structure in reflectance from biological tissue: a new technique for measuring nuclear size distribution," *Phys. Rev. Lett.* **80**, 627–630 (1998).
15. A. Wax, C. H. Yang, M. G. Muller, R. Nines, C. W. Boone, V. E. Steele, G. D. Stoner, R. R. Dasari, and M. S. Feld, "In situ detection of neoplastic transformation and chemopreventive effects in rat esophagus epithelium using angle-resolved low-coherence interferometry," *Cancer Res.* **63**, 3556–3559 (2003).
16. C. Loo, A. Lin, L. Hirsch, M. H. Lee, J. Barton, N. Halas, J. West, and R. Drezek, "Nanoshell-enabled photonics-based imaging and therapy of cancer," *Technol. Cancer Res. Treat.* **3**, 33–40 (2004).
17. A. Amelink, H. J. C. M. Sterenborg, M. P. L. Bard, and S. A. Burgers, "In vivo measurement of the local optical properties of tissue by use of differential path-length spectroscopy," *Opt. Lett.* **29**, 1087–1089 (2004).
18. A. Amelink and H. J. C. M. Sterenborg, "Measurement of the local optical properties of turbid media by differential path-length spectroscopy," *Appl. Opt.* **43**, 3048–3054 (2004).
19. L. Nieman, A. Myakov, J. Aaron, and K. Sokolov, "Optical sectioning using a fiber probe with an angled illumination-collection geometry: evaluation in engineered tissue phantoms," *Appl. Opt.* **43**, 1308–1319 (2004).
20. Y. L. Kim, Y. Liu, R. K. Wali, H. K. Roy, M. J. Goldberg, A. K. Kromin, K. Chen, and V. Backman, "Simultaneous measurement of angular and spectral properties of light scattering for characterization of tissue microarchitecture and its alteration in early precancer," *IEEE J. Sel. Top. Quantum Electron.* **9**, 243–256 (2003).
21. J. Yguerabide and E. E. Yguerabide, "Resonance light scattering particles as ultrasensitive labels for detection of analytes in a wide range of applications," *J. Cell Biochem. Suppl.* **37**, 71–81 (2001).
22. S. Schultz, D. R. Smith, J. J. Mock, and D. A. Schultz, "Single-target molecule detection with nonbleaching multicolor optical immunolabels," *Proc. Natl. Acad. Sci. U.S.A.* **97**, 996–1001 (2000).
23. S. J. Park, T. A. Taton, and C. A. Mirkin, "Array-based electrical detection of DNA with nanoparticle probes," *Science* **295**, 1503–1506 (2002).
24. S. L. Westcott, J. B. Jackson, C. Radloff, and N. J. Halas, "Relative contributions to the plasmon line shape of metal nanoshells," *Phys. Rev. B* **66**, 155431 (2002).
25. K. Sokolov, M. Follen, J. Aaron, I. Pavlova, A. Malpica, R. Lotan, and R. Richards-Kortum, "Real-time vital optical imaging of precancer using anti-epidermal growth factor receptor antibodies conjugated to gold nanoparticles," *Cancer Res.* **63**, 1999–2004 (2003).
26. Z. S. Wu and Y. P. Wang, "Electromagnetic scattering for multilayered sphere: recursive algorithms," *Radio Sci.* **26**, 1393–1401 (1991).
27. P. B. Johnson and R. W. Christy, "Optical constants of the noble metals," *Phys. Rev. B* **6**, 4370–4379 (1972).
28. J. F. Hillyer and R. M. Albrecht, "Gastrointestinal persorption and tissue distribution of differently sized colloidal gold nanoparticles," *J. Pharm. Sci.* **90**, 1927–1936 (2001).
29. G. F. Paciotti, L. Myer, D. Weinreich, D. Goia, N. Pavel, R. E. McLaughlin, and L. Tamarkin, "Colloidal gold: a novel nanoparticle vector for tumor directed drug delivery," *Drug Delivery* **11**, 169–183 (2004).
30. C. M. Goodman, C. D. McCusker, T. Yilmaz, and V. M. Rotello,

- “Toxicity of gold nanoparticles functionalized with Cationic and anionic side chains,” *Bioconjugate Chem.* **15**, 897–900 (2004).
31. R. Georgieva, R. Tsevi, K. Kosev, R. Kusheva, M. Balgijska, R. Petrova, V. Tenchova, I. Gitsov, and K. Troev, “Immobilization of aminosulfhydryl groups on poly(oxyalkylene phosphates). Formation of poly(oxyethylene phosphates)/cysteamine complexes and their radioprotective efficiency,” *J. Med. Chem.* **45**, 5797–5801 (2002).
  32. E. C. Dietze, A. Schafer, J. G. Omichinski, and S. D. Nelson, “Inactivation of glyceraldehyde-3-phosphate dehydrogenase by a reactive metabolite of acetaminophen and mass spectral characterization of an arylated active site peptide,” *Chem. Res. Toxicol.* **10**, 1097–1103 (1997).
  33. S. J. Oldenburg, R. D. Averitt, S. L. Westcott, and N. J. Halas, “Nanoengineering of optical resonances,” *Chem. Phys. Lett.* **288**, 243–247 (1998).
  34. J. Aizpurua, P. Hanarp, D. S. Sutherland, M. Kall, G. W. Bryant, and F. J. G. de Abajo, “Optical properties of gold nanorings,” *Phys. Rev. Lett.* **90**, 057401 (2003).
  35. K. L. Kelly, E. Coronado, L. L. Zhao, and G. C. Schatz, “The optical properties of metal nanoparticles: the influence of size, shape, and dielectric environment,” *J. Phys. Chem. B* **107**, 668–677 (2003).
  36. R. D. Averitt, S. L. Westcott, and H. J. Halas, “Linear optical properties of gold nanoshells,” *J. Opt. Soc. Am. B* **16**, 1824–1832 (1999).
  37. N. J. Halas, S. L. Westcott, S. J. Oldenburg, and T. R. Lee, “Controlled assembly of metal nanoparticle aggregates on silica nanoparticle surfaces,” *Abstr. Pap. - Am. Chem. Soc.* **218**, U423 (1999).
  38. J. B. Jackson and N. J. Halas, “Silver nanoshells: Variations in morphologies and optical properties,” *J. Phys. Chem. B* **105**, 2743–2746 (2001).
  39. L. M. Liz-Marzan, M. Giersig, and P. Mulvaney, “Synthesis of nano-sized gold-silica core-shell particles,” *Langmuir* **12**, 4329–4335 (1996).
  40. C. Radloff and N. J. Halas, “Enhanced thermal stability of silica-encapsulated metal nanoshells,” *Appl. Phys. Lett.* **79**(5), 674–676 (2001).
  41. S. P. Mulvaney, M. D. Musick, C. D. Keating, and M. J. Natan, “Glass-coated, analyte-tagged nanoparticles: a new tagging system based on detection with surface-enhanced Raman scattering,” *Langmuir* **19**(11), 4784–4790 (2003).
  42. M. Hu, X. Wang, G. V. Hartland, V. Salgueirino-Maceira, and L. M. Liz-Marzan, “Heat dissipation in gold-silica core-shell nanoparticles,” *Chem. Phys. Lett.* **372**(5–6), 767–772 (2003).
  43. R. T. Tom, A. Sreekumaran Nair, N. Singh, M. Aslam, C. L. Nagendra, R. Philip, K. Vijayamohan, and T. Pradeep, “Freely dispersible Au@TiO<sub>2</sub>, Au@ZrO<sub>2</sub>, Ag@TiO<sub>2</sub>, and Ag@ZrO<sub>2</sub> core-shell nanoparticles: one-step synthesis, characterization, spectroscopy, and optical limiting properties,” *Langmuir* **19**(8), 3439–3445 (2003).
  44. R. P. Bagwe, X. J. Zhao, and W. H. Tan, “Bioconjugated luminescent nanoparticles for biological applications,” *J. Dispersion Sci. Technol.* **24**(3–4), 453–464 (2003).
  45. M. Ming, Y. Chen, and A. Katz, “Synthesis and characterization of gold-silica nanoparticles incorporating a mercaptosilane core-shell interface,” *Langmuir* **18**(22), 8566–8572 (2002).
  46. F. Caruso, M. Spasova, V. Salgueirino-Maceira, and L. M. Liz-Marzan, “Multilayer assemblies of silica-encapsulated gold nanoparticles on decomposable colloid templates,” *Adv. Mater. (Weinheim, Ger.)* **13**(14), 1090 (2001).
  47. E. Prodan, C. Radloff, N. J. Halas, and P. Nordlander, “A hybridization model for the plasmon response of complex nanostructures,” *Science* **302**, 419–422 (2003).